[61] Martellucci, A. and Libby, P. A., "Supersonic Flow about General Three-Dimensional Blunt Bodies, Vol. II, Heat Transfer Due to the Interaction Between a Swept Planar Shock Wave and a Laminar Boundary Layer," ASD TR 61-727, Oct. 1962, Aeronautical Systems Div.

[62] Bogdonoff, S. M. and Vas, I. E., "A Preliminary Investigation of the Flow in a 90° Corner at Hypersonic Speeds, Part I—Flat Plates with their Leading Edges at Zero Angle of Attack," TR 57-202, Dec. 1957, Air Research and Development Command.

[63] Stainback, P. C., "Heat Transfer Measurements at a Mach Number of 8 in the Vicinity of a 90° Interior Corner Aligned with the Free-Stream Velocity," TN D-2417, Aug. 1964, NASA.

[64] Stainback, P. C., "An Experimental Investigation at a Mach Number of 4.95 of Flow in the Vicinity of a 90° Interior Corner Aligned with the Free-Stream Velocity," TN D-184, Feb. 1960, NASA.

[65] Cresci, R. J. et al., "Hypersonic Interaction Along a Rectangular Corner," *AIAA Journal*, Vol. 7, No. 12, Dec. 1969, pp. 2241–2246; see also Papers 14 and 18 *AGARD Conference Proceedings* No. 30, May 1968.

[66] Cresci, R. J., "Hypersonic Flow Along Two Intersecting Planes," *Proceedings 1966 Heat Transfer and Fluid Mechanics Institute*, Stanford University Press, pp. 357–365.

[67] Charwat, A. F. and Redekopp, L. G., "Supersonic Interference Flow Along the Corner of Intersecting Wedges," *AIAA Journal*, Vol. 5, No. 3, March 1967, pp. 480–488.

[68] Stainback, P. C. and Weinstein, L. M.; "Aerodynamic Heating in the Vicinity of Corners at Hypersonic Speeds," TN D-4130, Nov. 1967, NASA.

[69] Watson, R. D. and Weinstein, L. M., "A Study of Hypersonic Corner Flow Interactions," AIAA Paper 70-227, New York, 1970.

[70] Goebel, T. P., "A Theoretical Study of Inviscid Supersonic Flow along a Corner Formed by the Intersection of Two Wedges," Ph.D. thesis, 1969, Univ. of California, Los Angeles.

[71] Hayes, W. D. and Probstein, R. F., *Hypersonic Flow Theory*, 2nd ed., Vol. I. Academic Press, New York, 1966, p. 223.

[72] Newlander, R. A., "Effect of Shock Impingement on the Distribution of Heat Transfer Coefficients on a Right Circular Cylinder at Mach Numbers of 2.65, 3.51, and 4.44," TN D-642, Jan. 1961, NASA.

[73] Gulbran, C. E. et al., "Heating in Regions of Interfering Flow Fields—Part II: Leading Edge Shock Impingement," AFFDL TR 65-49, Jan. 1967, Pt. II, Air Force Flight Dynamics Lab.

[74] Ray, A. D. and Palko, R. L., "An Investigation of the Effects of Shock Impingement on a Blunt Leading Edge," AEDC TR 65-153, 1965, Arnold Engineering Development Center.

[75] Bushnell, D. M., "Effects of Shock Impingement and other Factors on Leading Edge Heat Transfer," TN D-4543, April 1968, NASA.

[76] Edney, B. E., "Anomalous Heat Transfer and Pressure Distributions on Blunt Bodies at Hypersonic Speeds in the Presence of an Impinging Shock," Rept. 115, The Aeronautical Research Institute of Sweden, Stockholm, Sweden, Feb. 1968; also "Effects of Shock Impingement on the Heat Transfer around Blunt Bodies," *AIAA Journal*, Vol. 6, No. 1, Jan. 1968, pp. 15–21.

MAY 1971 AIAA JOURNAL VOL. 9, NO. 5

Theoretical Analysis of Vortex Shedding from Bodies of Revolution in Coning Motion

G. D. KUHN,* S. B. SPANGLER,† AND J. N. NIELSEN‡
Nielsen Engineering & Research Inc., Mountain View, Calif.

A theoretical flow model for the steady asymmetric vortex system shed from a slender body in coning motion is described. The model was developed using potential flow methods and slender-body theory, and provides for the calculation of the strengths and positions of two unequal concentrated vortices and the resulting force distribution induced on the body. The vortex motion is determined in the flowfield which consists of a portion described by a velocity potential plus a portion due to rotation. The method of determining the initial conditions for the vortex motions is discussed. Comparisons are made between predicted and experimental values of side forces and side moments for slender cones and ogive-cylinder combinations in lunar coning motion.

Introduction

THE nature of vortex formation on an inclined slender body and its relation to the two-dimensional flow over a cylinder was recognized some 20 years ago.[1] Since then a considerable amount of effort has been expended in studying the nature of the flow over such bodies and the vortex-induced force distribution on them.[2,3] It has been only recently, however, that the presence of a steady vortex pair on a slender body in a coning motion has been established.[4] The work described in this paper is a theoretical analysis of that problem. The work was reported in detail in Ref. 5.

The coning problem is of importance for spinning bodies which encounter a pitch-roll resonance condition, from which a lunar coning motion (roll lock-in) can develop with unacceptably high angles of attack. The reasons for the development of this type of motion are not well understood. Tobak[4] has developed a formulation for the aerodynamic moment system in lunar motion which does not depend on constructing the nonplanar motion as the sum of two planar motions. This approach permits coupling of the two planar motions and identifies two types of "Magnus moments": one due to spin about the body axis and one due to rotation of the angle of attack plane (the plane formed by the wind vector and the body axis). The existence of vortices over the body provides a potential source of coupling and nonlinear moments of the latter type.

Presented as Paper 70-52 at the AIAA 8th Aerospace Sciences Meeting, New York, January 19–21, 1970; submitted March 4, 1970; revision received June 29, 1970.

This work was supported by NASA Ames Research Center, under Contract NAS2-4765.

* Research Scientist. Member AIAA.
† Vice President. Member AIAA.
‡ President. Fellow AIAA.

Problem Description

A sketch of the motion being considered is shown in Fig. 1. The analysis of the motion is based on the following assumptions:

1) The body center of gravity traverses a straight path at constant velocity V through a constant density fluid.

2) The body axis is inclined at a fixed angle, α, with the direction of motion of the center of gravity. The body undergoes a coning motion in which the angle of attack plane rotates at constant angular velocity ω, about the velocity vector.

3) The body spins at the rate ω (lunar motion).

4) A steady vortex pair exists over the leeward side of the body.

Basic Approach

In the real flow, vortex sheets emanate from the separation lines and roll up over the leeward side of the body to form two regions of concentrated vorticity (Fig. 1). In the theoretical approach, the two regions of concentrated vorticity over the body are replaced by two potential vortex filaments. The steady three-dimensional potential flow problem is then solved through the use of slender-body theory. The analysis is carried out as the unsteady two-dimensional flow in a plane fixed in the fluid and normal to the flight velocity vector.

In the fixed plane, a rotating y,z axis system is defined, where the origin of the axis is the center of the circle representing the body cross section in the plane and the z axis lies in the angle-of-attack plane. The body nose is considered to pierce the fixed plane at $t = 0$. Thus, the angle-of-attack plane makes an angle ωt with the x',z' plane.§ The two vortex filaments originate at the nose and move away from the body and grow in strength with distance along the body.

The flow model in the fixed plane appears as shown in Fig. 2. The y',z' axes shown are projections of the inertial y',z' axes into the plane. If all motion is taken with respect to the y,z coordinate system, then there exists a fluid velocity along the positive y axis (horizontal crossflow) proportional to ω and a fluid velocity along the z axis (vertical crossflow) of magnitude $V\alpha$.¶ In addition there is a solid body rotation of the fluid past the body so that the flowfield in the y,z system is rotational. In keeping with the small angle assumption, the body cross sections in the fixed plane are assumed circular to first order.

The vortices are considered to be fed from points ζ_{0j} on the body, which are the locations of the separation lines on the flanks of the body. The separation points are assumed to have fixed angular relationships with respect to the resultant crossflow vector [vector sum of $V\alpha$ and $\omega V\alpha(t_{cg} - t)$] so that they and the crossflow vector rotate with respect to the y,z system at the same angular rate. The vortex strength at a given vortex position is determined from the condition that the velocity at ζ_0 is zero relative to the separation point. The vortex velocity is determined from a condition of zero net force on the vortex and its "feeding sheet," a line connecting the vortex to the separation point along which vorticity is considered to be transported.

Formulation in the Rotating Coordinate System

In the y',z' coordinate system, the fluid is irrotational and is at rest at infinity. Thus, the flowfield satisfies Laplace's equation and a velocity potential exists.

The absolute velocity of a point in a fluid is equal to the velocity relative to a moving coordinate system plus the velocity of the moving system. Thus, the fluid velocity relative to the y,z coordinate system consists of an irrotational part, derivable from a potential, plus a rotational part. The fluid velocity in the rotating system is

$$v - iw = -iV\alpha(1 + a^2/\zeta^2) - \omega V\alpha(t_{cg} - t)(1 - a^2/\zeta^2) + a\dot{a}/\zeta - i\lambda_1[1/(\zeta - \zeta_{v1}) - 1/(\zeta - a^2/\bar{\zeta}_{v1})] - i\lambda_2[1/(\zeta - \zeta_{v2}) - 1/(\zeta - a^2/\bar{\zeta}_{v2})] - i\omega\bar{\zeta} \quad (1)$$

where $\zeta = y + iz$, $\lambda = \Gamma/2\pi$, and Γ represents the strength of a vortex.** The first two terms in Eq. (1) represent the crossflow. The third term is a source representing the fact that the body radius is changing with time. The fourth and fifth terms of Eq. (1) represent the velocity due to the two external vortices and their images. The assumption has been made in this work that the net circulation in the plane fixed in the fluid should always be zero. The last term in Eq. (1) accounts for the rotation of the coordinate system.

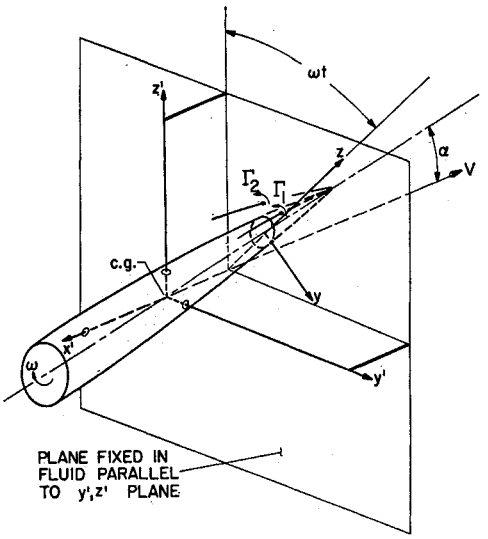

Fig. 1 Sketch of the motion of the body through the fluid.

Solution for Vortex Motion and Strengths

The condition that the fluid velocities relative to the moving separation points at ζ_{01} and ζ_{02} are zero,

$$\{v - iw\}_{\zeta_j = \zeta_{0j}} = \dot{\bar{\zeta}}_{0j} \qquad j = 1,2 \quad (2)$$

supplies two algebraic equations for the two unknowns Γ_1 and Γ_2.

The condition for zero net force on a vortex and its "feeding sheet" is formulated by observing that the force on the ex-

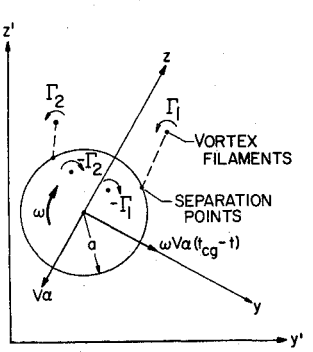

Fig. 2 Flowfield in the plane fixed in the fluid.

§ The x',y',z' system is a nonrotating coordinate system fixed at the body center of gravity.

¶ The assumption is made in the analysis that trigonometric functions of α can be approximated with sufficient accuracy by small angle relations; that is, $\sin\alpha \cong \tan\alpha \cong \alpha$, and $\cos\alpha \cong 1$.

** In the mathematical formulation, the sign convention on Γ is such that Γ is positive for a counter-clockwise rotating vortex when viewed in the coordinate system shown in Fig. 2.

ternal vortex is equal and opposite to that on the "sheet." The force on an external vortex is $i\rho\Gamma(\dot{\bar{\zeta}}_v - V_v)$, where V_v is the velocity induced at the vortex by all components of the flow other than the vortex itself, and $\dot{\bar{\zeta}}_v - V_v$ is the vortex velocity relative to the local induced flow. The force on the sheet is determined from the unsteady Bernoulli equation applied to the irrotational flow around a vortex. This yields the pressure difference across the feeding sheet as $\rho\Gamma$. The net force on the sheet is then the product of the pressure difference across the sheet and the length of the sheet.

Thus, the force balance relation for each vortex is

$$i\rho\Gamma_j(\dot{\bar{\zeta}}_{vj} - V_{vj}) + i\rho\dot{\Gamma}_j(\zeta_{vj} - \zeta_{0j}) = 0 \qquad j = 1,2 \quad (3)$$

The only unknown is the vortex velocity $\dot{\bar{\zeta}}_{vj}$. Equations (1–3), after some algebra, yield a set of simultaneous first-order differential equations, linear in the derivatives, $\dot{\bar{\zeta}}_{vj}$. The differential equations and their derivation are presented in more detail in Ref. 5.

The equations for the vortex motion are to be solved for given initial values. The vortices cannot be started on the body because the feeding points are singularities. The determination of the vortex motion in the immediate vicinity of the feeding points was examined by expanding the equations in Taylor series in terms of the vortex displacement from the feeding points. The expansion yielded the trajectories along which the vortices move in the near vicinity of the feeding points, but could provide no information about the relation of the initial displacements of the two vortices. The feeding points were shown to be unstable saddle points with a single integral curve passing through each, inclined at an angle of 30° to the downstream tangent to the body at the feeding point. This result is identical to that of Bryson[6] for the case of planar motion. However, unlike the planar motion problem, the a priori assumption of symmetry of initial vortex displacement is not justified in this case. The analysis of the initial motion is described in more detail in Ref. 5. In order to determine if the initial displacements of the two vortices could be connected using some property of their asymptotic downstream behavior, the motion of the vortices far from the body was examined. This behavior will be described in a subsequent section.

In order to integrate the differential equations for the vortex motion, the angle arguments of ζ_{0_1} and ζ_{0_2} must first be selected. Data on separation line location for the planar motion case at moderate angles of attack indicate the separation lines on the two flanks of the body to be symmetrical about a vertical plane through the body axis. For the lunar coning case where no data are available as a guide, the most reasonable first approximation is to assume that the separation lines are located symmetrically with respect to the resultant crossflow vector. Since the $\omega V\alpha(t_{cg} - t)$ component varies with time (or distance along the body) and its direction changes at t_{cg}, the resultant crossflow vector will rotate in the y,z system with increasing time.

Calculation of Forces and Moments

The force distribution on the body was calculated by using the Bernoulli equation to obtain the pressure distribution, which was then integrated to obtain the force. In the nonrotating y',z' coordinate system, the force per unit length can be expressed as

$$\frac{dF'}{dx} = \frac{dY'}{dx} + i\frac{dZ'}{dx} = -e^{-i\omega t}\rho\int_c \frac{p}{\rho}d\zeta \qquad (4)$$

where the contour c is the periphery of the circle representing the body, and the body nose is considered to pierce the plane fixed in the fluid (at $t = 0$) with the imaginary axes of the fixed (ζ') and rotating (ζ) coordinate systems aligned.

While the calculation of vortex motion can be accomplished in the rotating, ζ, coordinate system, some care must be exercised in distinguishing between the two axis systems in carrying out the force computation. In the ζ' system, the flow is completely irrotational and all fluid velocities are zero at an infinite distance from the body. A velocity potential $\phi'(\zeta',t)$ exists, which is the real part of $W'(\zeta',t)$, given as follows:

$$W'(\zeta',t) = V\alpha[i - \omega(t_{cg} - t)](a^2/A) + a\dot{a}\ln A - i\lambda_1\ln[e^{i\omega t}(\zeta' - \zeta_{v_1}')/B_1] - i\lambda_2\ln[e^{i\omega t}(\zeta' - \zeta_{v_2}')/B_2] \quad (5)$$

where

$$A = \zeta' e^{i\omega t} - iV\alpha(t_{cg} - t)$$

and

$$B_j = A - a^2/[\bar{\zeta}_{vj}'e^{-i\omega t} + iV\alpha(t_{cg} - t)] \qquad j = 1,2$$

The Bernoulli equation for unsteady flow in the ζ' system is given by paragraph 3.60 of Ref. 7 as

$$\frac{p}{\rho} = -\frac{\partial\phi'(\zeta',t)}{\partial t} - \frac{1}{2}(v'^2 + w'^2) + C(t) \qquad (6)$$

where the constant C is uniform throughout the flow at a given instant of time. The procedure is to obtain the proper forms of the first two terms on the right-hand side of Eq. (6) using the real part of Eq. (5) for $\phi'(\zeta',t)$ and the derivative of Eq. (5), $dW'(\zeta',t)/d\zeta'$ for $v' - iw'$. The contour integration indicated in Eq. (4) is then performed. With respect to the integration, it is noted in Ref. 8 for the case of free vortices external to a body that the contour can be enlarged from the body periphery to a contour of infinite radius since inclusion of the force-free vortices within the contour will not change the computed force. The same is true in the present case since the vortices plus their feeding sheets are force-free. The only term that contributes in Eq. (4) is the time derivative of the velocity potential.

The application of this approach to the problem results in the following expression for the force per unit length,

$$dF'/dx = e^{-i\omega t}\{2\pi\rho a\dot{a}V\alpha[i - \omega(t_{cg} - t)] + \pi a^2\rho\omega V\alpha[2 + i\omega(t_{cg} - t)] + \rho\omega[\Gamma_1(\zeta_{v_1} - a^2/\bar{\zeta}_{v_1}) + \Gamma_2(\zeta_{v_2} - a^2/\bar{\zeta}_{v_2})] + \partial/\partial t[i\rho\Gamma_1\zeta_{v_1}(1 - a^2/r_{v_1}^2)] + \partial/\partial t[i\rho\Gamma_2\zeta_{v_2}(1 - a^2/r_{v_2}^2)]\} \quad (7)$$

where

$$r_{vj} = [\zeta_{vj}\bar{\zeta}_{vj}]^{1/2}$$

The first two terms represent forces that are derived from the attached flow around the body due to the body radius changing with axial distance and the cross-coupling between the rotational and angle-of-attack motions. The next term arises from the motion of the vortices in the rotational flow around the body. The last two terms represent the time rate of change of impulse of each external vortex and its image, and are identical to the terms that occur for the planar motion case.

Computer Program for Vortex Motion and Forces on Body

The differential equations which must be solved for the vortex motion are a set of first-order ordinary differential equations, linear in the derivatives. The expressions for the

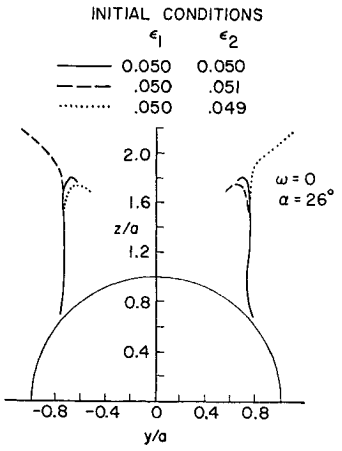

Fig. 3 Vortex trajectories on a cylindrical body in planar motion for different initial conditions, $\alpha = 26°$, $\omega l_{cg}/V = 0.0$.

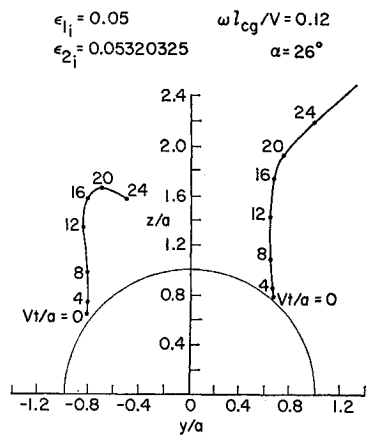

Fig. 4 Vortex trajectories on a cylindrical body in coning motion for symmetrical initial conditions, $\epsilon_{1_i} = \epsilon_{2_i} = 0.05$, $\omega l_{cg}/V = 0.12$.

force and the moments about the center of gravity of the body are of the same form.

Integration of the differential equations and the forces and moments is accomplished using a fourth-order Adams-Moulton predictor-corrector method[9] with starting values determined using a Runge-Kutta integration scheme. Initial values of ζ_1, ζ_2, and t are provided as input to the computer program.

Effect of Initial Conditions on Asymptotic Vortex Behavior

Cylindrical Bodies

An investigation was conducted to determine the sensitivity of the downstream behavior of a pair of vortices on the leeward side of a cylindrical body. The initial vortex positions were defined as

$$\zeta_{vj} = \zeta_{0j} + a\epsilon_j e^{i\phi_j}$$

The values of ϵ_j were provided as input to the computer program, along with the body radius and the locations of the feeding points. The angles ϕ_j were computed from the first-order analysis mentioned previously. The initial location of the right-hand vortex, ϵ_1, was always specified as 0.05 whereas the initial value of ϵ_2 was varied.

Nonconing case

The first step in the study of the downstream behavior was to examine the case of planar motion ($\omega = 0$) both with symmetrical initial values of ϵ and with small deviations from initial symmetry to gain insight into the effect of initial errors on the downstream behavior. Some results are shown in Fig. 3 for the case of $\alpha = 26°$ and $\theta_s = 50°$ with separation considered to originate at $t = 0$. Figure 3 shows the trajectories of the vortices for initial values of ϵ_2 of 0.049, 0.05, and 0.051. For the case of symmetrical initial positions, the vortices pass outside of and then curve in to asymptotically approach points at which the vortex strengths and positions become constant. These points are the Föppl points defined as the positions where, for a particular vortex strength, the resultant velocities at the vortices are zero. Since the vortex strengths in the present problem are determined by the locations of the separation points on the body, the Föppl points are uniquely determined. For unsymmetrical initial positions the Föppl point is never reached, as shown by the dashed curves of Fig. 3.

It is characteristic of the symmetrical planar motion solution that the vortex strength will increase to a point about 30 radii downstream of the nose, at which point the vortex begins to curve towards the Föppl point and the vortex strength begins to decrease; that is, $\dot{\Gamma}$ becomes negative. At this point, the solution becomes physically unrealistic since the occurrence of negative $\dot{\Gamma}$ implies that vorticity is being fed back into the body boundary layer rather than being shed from the boundary layer. This may mean that the feeding sheet is actually broken, which could result in the freeing of one of the vortices and formation of an asymmetric vortex configuration.

Coning case

One would expect to find with coning motion a downstream behavior of the vortices similar to that of the planar motion case, at least for small coning rates. This result is illustrated in Figs. 4 and 5 for the case of $\omega l_{cg}/V = 0.12$ and $\epsilon_{1_i} = 0.05$. Several calculations were made for different values of ϵ_{2_i}. The results for $\epsilon_{2_i} = 0.05$ are shown in Fig. 4, while the results for $\epsilon_{2_i} = 0.05320325$ are shown in Fig. 5. The behavior shown here is qualitatively similar to that shown for the nonconing case, as shown in Fig. 3. Figures 4 and 5 indicate that the two vortices move away from their feeding points at similar rates. In Fig. 4, a situation similar to that of Fig. 3 for unsymmetrical initial conditions is found. For the initial conditions of Fig. 5, the result is similar to the symmetrical case of Fig. 3. The vortices first accelerate, then slow and finally approach positions that are essentially stationary with respect to the resultant crossflow vector. Furthermore, for the case of Fig. 5, $\dot{\Gamma}$ becomes negative for both vortices at approximately 30 radii downstream as in the planar motion case. Thus, the downstream behavior of the vortices with coning motion is qualitatively the same as that for the planar motion, at least for moderate coning rates.

The principal vortex-induced force distribution is in the z direction. The side-force distribution is an order of magnitude lower and is quite sensitive to the difference in vortex positions and strengths caused by small differences in initial conditions. For example, with $\epsilon_{1_i} = 0.05$, a value of $\epsilon_{2_i} = 0.05$ produces a large side force to leeward, whereas values of ϵ_{2_i} of 0.054 and 0.05320325 produce small side forces to windward. These results indicate the importance of obtaining a reliable method for determining initial conditions.

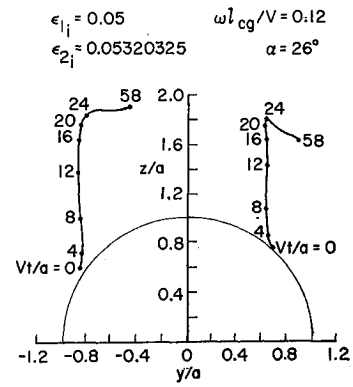

Fig. 5 Vortex trajectories on a cylindrical body in coning motion for unsymmetrical initial displacements; $\epsilon_{1_i} = 0.05$, $\epsilon_{2_i} = 0.05320325$, $\omega l_{cg}/V = 0.12$, $\alpha = 26°$.

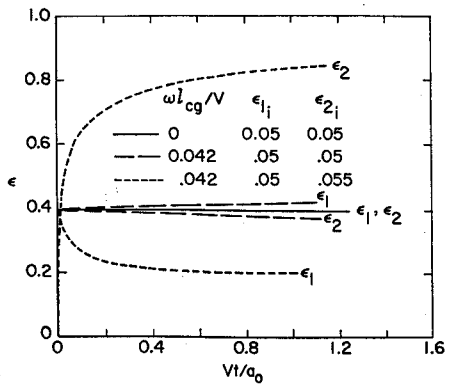

Fig. 6 Nondimensional vortex displacement on a 10° half-angle cone at 34° angle of attack; feed-points at 34° from resultant crossflow vector.

Conical Bodies

For the case of a slender cone at angle of attack with flow separation and vortex formation, Bryson[6] derived the vortex motion and forces on the assumption that the flowfield is conical. Thus, solutions in the crossflow planes are similar and are scaled according to distance from the cone vertex. The present formulation of the problem does not employ such an assumption. Consequently, a number of calculations were made with conical bodies to check the Bryson results for the planar motion case and to determine the nature of the present solution for the coning case.

The behavior of the vortices shed from a slender cone for both planar and coning motion is shown in Fig. 6. The configuration is a 10° half-angle cone of length l_0 and base radius a_0 with the center of gravity at $l_{cg}/l_0 = 0.61$ for the coning case. The cone angle of attack is 34°. In both cases, the separation lines were specified at angles, θ_s, 34° from the resultant crossflow vector. The initial conditions are indicated on the figure. The starting positions of the vortices were specified on lines in the crossflow plane inclined 30° to the downstream tangents to the body at the feeding points. The variation of ϵ_1 and ϵ_2 for planar motion ($\omega = 0$) is indicated in Fig. 6 by a solid line, while the broken lines represent the variation for $\omega l_{cg}/V = 0.042$. The vortices in all cases were started at $x/l_0 = 0.0191$. For the $\omega = 0$ case, the solution immediately converges to a value of $\epsilon = 0.3976$ with the vortices on lines 36.86° from the downstream tangents to the body at the feeding points.

In the coning case, the asymptotic solution is very sensitive to the initial conditions just as it is for the cylindrical body. For equal initial values of ϵ_1 and ϵ_2, the solution converges very rapidly in the same manner as the planar motion case, but the asymptotic solution is one in which ϵ_1 increases approximately linearly with time and ϵ_2 decreases. For ϵ_2 = 0.055, the downstream solution is characterized by even greater asymmetry.

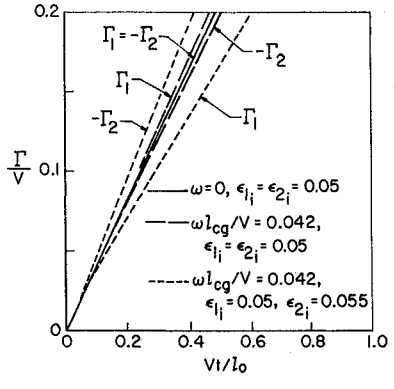

Fig. 7 Variation of vortex strengths for planar and coning motion of a 10° half-angle cone at 34° angle of attack.

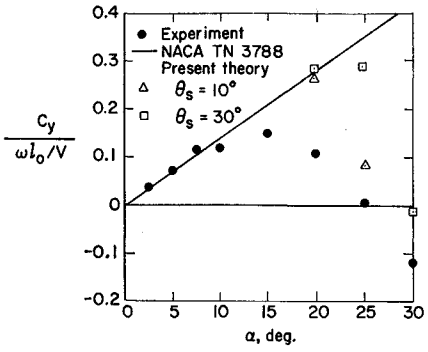

Fig. 8 Side-force coefficient on 10° half-angle cone due to coning motion; $M_\infty = 2.0$, $l_{cg}/l_0 = 0.61$.

Of the two sets of results for coning motion shown in Fig. 6, the set using symmetric initial conditions is the most plausible. In the planar motion case where the initial conditions and the locations of the separation lines are clearly symmetrical, a conical solution is obtained, which implies that the vortices originate on the axis of the cone at its apex. For the coning motion case, the vortices should also originate on the cone axis at the apex. At the apex, the velocity due to the rotational flowfield, which is the principal source of asymmetrical growth and motion of the vortices, is zero. Thus, the initial vortex motion and growth at the cone apex should resemble that of the planar motion case.

The results for the vortex strengths are shown in Fig. 7. In the planar motion case, the vortex strengths are equal and increase linearly with time, or distance along the body. In the coning case, the strengths still increase linearly with time, but at different rates.

Comparisons with Data

Slender Cones

Unpublished data on a 10° half-angle cone were obtained from the NASA Ames Research Center. The cone was mounted on a bent sting such that the sting could be rotated to produce the coning motion and the cone could be spun relative to the sting. The angle of attack could be varied using interchangeable stings. A six-component force balance system measured aerodynamic forces in body coordinates and moments about the center of gravity. Photographs were taken of the vortex positions at various axial stations using the vapor screen technique and a camera mounted on the rotating sting. The cone was mounted with its center of gravity at the 61% length station. The tests were conducted in the 6- × 6-Foot Wind Tunnel at a Mach number of 2.0.

In comparing the forces and moments on the cone, it is useful to consider the forces due to both the attached and the separated flow around the body. The work of Ref. 10 predicts a linear variation of the total side force coefficient and the total side moment coefficient with angle of attack. Figure 8 shows the comparison between theory and data for the variation of side-force coefficient, $C_y/(\omega l_0/V)$, with angle of attack. The present theory is indicated by open symbols while the experiment is indicated by filled circles. Theoretical results for two values of the separation line location, θ_s, are shown. The linear variation of $C_y/(\omega l_0/V)$ for small angles of attack is predicted very well by the results of Ref. 10 as shown in the figure. The predicted values at high angles of attack were obtained by adding to the linear variation for attached flow, the predicted nonlinear contributions due to the vortices. In Fig. 9 the theoretical side moment on the cone is compared with the experimental data in the same manner as for the aforementioned force coefficient.

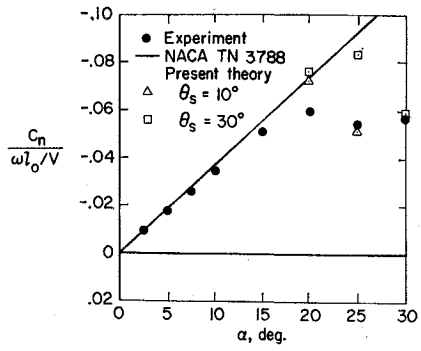

Fig. 9 Side-moment coefficient on 10° half-angle cone due to coning motion; $M_\infty = 2.0$, $l_{cg}/l_o = 0.61$.

Figures 8 and 9 indicate that the predicted results are strongly influenced by the location of the vortex feeding points. For a given value of θ_s, the vortex-induced side force first appears at a larger angle of attack than the data indicate and increases at a faster rate than the data as the angle of attack is increased. The figures indicate that it may be possible to improve the prediction of the side force if θ_s is varied with angle of attack. This result is in qualitative agreement with the data of Ref. 11, where the angle of separation, θ_s, on inclined bodies in planar motion is shown to depend strongly on angle of attack. Also, it may be necessary to specify an axial variation of the separation line location different from the constant angular displacement from the resultant crossflow vector as used in the present theory. It is apparent that knowledge of the separation line location is an important factor in developing a predictive technique.

Ogive-Cylinders

Some experimental measurements of side moments on a slender ogive-cylinder body are presented in Ref. 4. As in the cone experiments, vapor screen photographs were used to observe the vortices. The total side moment ahead of the center of gravity was measured. The configuration is a cylinder 2.5 in. in diameter ($a_0 = 1.25$ in.) with a fineness-ratio 3.4 tangent-ogive nose. The center of gravity was 2.5 ft from the nose of the body. The tests were run in the

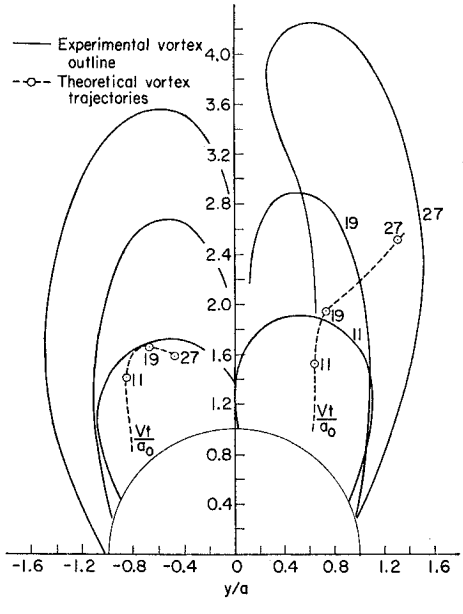

Fig. 10 Comparison of theoretical and experimental vortex trajectories on an ogive-cylinder body in coning motion; $\omega l_{cg}/V = 0.12$, $\alpha = 26°$.

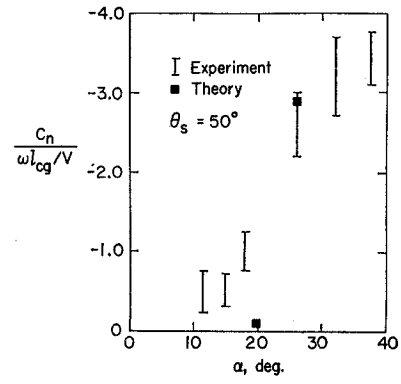

Fig. 11 Side-moment coefficient on a slender ogive-cylinder.

Ames Research Center 6- × 6-Foot Wind Tunnel at a Mach number of 1.4 and freestream unit Reynolds number of about 2.0×10^6/ft.

Theoretical calculations of the vortex-induced forces on the ogive cylinder were made based on the assumption that the vortices started on the ogive nose of the body. Initial vortex positions were obtained from calculations for a cone based on the conclusion reached previously that a unique set of initial conditions can be obtained for the solution for a cone. The separation points were each assumed to be at angles, θ_s, 50° from the resultant crossflow vector, which value corresponds to measured separation line locations on ogive-cylinders and cone-cylinders at angle of attack.[11] The angle of 50° was chosen as the best estimate of an average value of the angular location of the separation line since the location actually varies along the body, whereas the computer program used here can only handle constant values of θ_s. The asymptotic solution for the vortex trajectories on the cone was then used to obtain the positions of the vortices on the ogive at the station at which the ogive was tangent to the 10° cone. The angle of 10° for the cone was chosen arbitrarily.

The results for the predicted vortex positions for an angle of attack of 26° and a coning rate ($\omega l_{cg}/V$) of 0.12 are compared with sketches made from unpublished vapor screen photographs for three axial stations in Fig. 10. While the "centers" of the areas of concentrated vorticity are difficult to determine, the predicted vortex positions tend to agree qualitatively with the photographic information. The theory predicts that the right-hand vortex is further away from the body than the left-hand vortex. The right-hand vortex has a greater strength than the left-hand vortex until a point about 10 radii from the nose, beyond which the strength of the left-hand vortex becomes larger.

The side-moment coefficient on the portion of the body from the nose back to the center of gravity is attributable almost entirely to the vortex-induced side-force distribution. This conclusion is substantiated by the data presented in Ref. 4, which is reproduced as Fig. 11. The predicted side moment is a strong function of the separation angle as it was for the cone. However, a predicted value for 26°, shown in Fig. 11, indicates the correct magnitude. In the tests just described, photographs of the vortex positions were obtained up to 8 diam aft of the center of gravity. Sketches of the areas of concentrated vorticity for $\alpha = 25°$ and $\omega l_{cg}/V = 0.12$ are

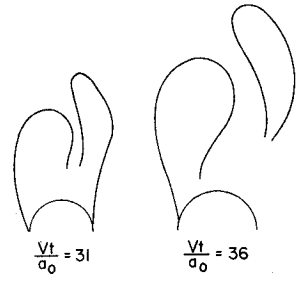

Fig. 12 Sketches of vortices on ogive-cylinder in coning motion from vapor screen photographs, $\omega l_{cg}/V = 0.12$, $\alpha = 25°$.

shown in Fig. 12. Near the aft end of the body, the photographs tend to indicate that the right-hand vortex becomes free, much as occurs on long slender bodies in planar motion at high angles of attack. Theoretical solutions for the ogive-cylinder indicate that $\dot{\Gamma}$ can become negative for certain combinations of initial conditions, angle of attack, coning rate, and separation line locations. Such behavior suggests that the tearing of the feeding sheet of one vortex might occur at the point where $\dot{\Gamma}$ becomes negative, and a new bound vortex would be started at the separation point. No calculations have been made along these lines at the present time.

Concluding Remarks

Based on experimental evidence of the existence of a steady asymmetric vortex system on a slender body in coning motion, a theoretical flow model for vortex shedding was developed using potential flow methods and slender-body theory. The model provides for the calculation of the strength and position of each of the two vortices representing the areas of concentrated vorticity and the resulting force distribution induced on the body. The results for vortex motion and forces were found to be quite sensitive to the initial asymmetry. Upon specializing the body to a cone, it was found that the full nonlinear solution rapidly converged to a unique solution.

On the basis of agreement with data for a cone and an ogive-cylinder in lunar coning motion, the flow model developed herein is felt to describe reasonably accurately the nature of the vortex-like separated flow over the body and the vortex-induced force distribution. The vortex flow is shown to produce a side force to leeward and a stabilizing side moment in correspondence with the measured results.

The theoretical solution depends on assumptions regarding the separation line location. For the lunar motion case, the body is not spinning relative to the boundary layer, so that use of separation location data obtained for planar motion should be a reasonable assumption. The development of a truly predictive method requires a three-dimensional boundary-layer solution that would predict the location of the separation lines over the length of the body and the initial positions and strengths of the vortices. Such a method would then permit calculation of the general case of coning motion with nonlunar spin rates.

Finally, the nature of the theoretical solution suggests the possibility of predicting the asymmetric vortex pattern developed at high angles of attack. The theoretical results indicate that at some station aft along the body, the rate of change of strength of the windward vortex can approach zero or go negative, which suggests that since vorticity would no longer be fed to the vortex from the separation line, the sheet should be cut. This result is in accordance with experimental observations of vortex flow over bodies at relatively high angles of attack, which tend to indicate the existence of a steady asymmetric vortex pattern, with sheets being torn and free vortices formed.

References

[1] Allen, H. J. and Perkins, E. W., "A Study of Effects of Viscosity on Flow over Slender Inclined Bodies of Revolution," Rept. 1048, 1951, NACA.

[2] Mello, J. F., "Investigation of Normal Force Distribution and Wake Vortex Characteristics of Bodies of Revolution at Supersonic Speeds," *Journal of the Aeronautical Sciences*, Vol. 26, No. 3, March 1959, pp. 155–168.

[3] Perkins, E. W. and Jorgensen, L. H., "Comparison of Experimental and Theoretical Normal Force Distribution on an Ogive Cylinder Body at M = 1.98," TN 3716, 1956, NACA.

[4] Tobak, M., Schiff, L. B., and Peterson, V. L., "Aerodynamics of Bodies of Revolution in Nonplanar Motion," *AIAA Journal*, Vol. 7, No. 1, Jan. 1969, pp. 75–82.

[5] Kuhn, G. D., Spangler, S. B., and Nielsen, J. N., "Theoretical Study of Vortex Shedding from Bodies of Revolution Undergoing Coning Motion," CR-1448, Oct. 1969, NASA.

[6] Bryson, A. E., "Symmetric Vortex Separation on Circular Cylinders and Cones," *Journal of Applied Mechanics*, Vol. 26, No. No. 4, Dec. 1959, pp. 643–648.

[7] Milne-Thomson, L. M., "Irrotational Motion Pressure Equation," *Theoretical Hydrodynamics*, 4th ed., MacMillan, New York, 1960, p. 86.

[8] Sacks, A. H., "Vortex Interference on Slender Airplanes," TN 3525, Nov. 1955, NACA.

[9] Hildebrand, F. B., *Introduction to Numerical Analysis*, McGraw-Hill, New York, 1956, pp. 198–199.

[10] Tobak, M. and Wehrend, W. R., "Stability Derivatives of Cones at Supersonic Speeds," TN 3788, Sept. 1956, NACA.

[11] Spangler, S. B., Sacks, A. H., and Nielsen, J. N., "The Effect of Flow Separation from the Hull on the Stability of a High-Speed Submarine. Part I. Theory," Rept. 107, Aug. 15, 1963, Vidya, Palo Alto, Calif.